



Relative sea-level change in Connecticut (USA) during the last 2200 yrs



Andrew C. Kemp^{a,*}, Andrea D. Hawkes^b, Jeffrey P. Donnelly^c, Christopher H. Vane^d, Benjamin P. Horton^{e,f,g}, Troy D. Hill^h, Shimon C. Anisfeld^h, Andrew C. Parnellⁱ, Niamh Cahillⁱ

^a Department of Earth and Ocean Sciences, Tufts University, Medford, MA 02155, USA

^b Department of Geography and Geology, University of North Carolina Wilmington, Wilmington, NC 28403, USA

^c Department of Geology and Geophysics, Woods Hole Oceanographic Institution, Woods Hole, MA 02543, USA

^d British Geological Survey, Center for Environmental Geochemistry, Keyworth, Nottingham, NG12 5GG, UK

^e Sea Level Research, Department of Marine and Coastal Sciences, Rutgers University, New Brunswick, NJ 08901, USA

^f Institute of Earth, Ocean and Atmospheric Sciences, Rutgers University, New Brunswick, NJ 08901, USA

^g Earth Observatory of Singapore and Asian School of the Environment, Nanyang Technological University, 639798, Singapore

^h School of Forestry and Environmental Studies, Yale University, New Haven, CT 06511, USA

ⁱ School of Mathematical Sciences (Statistics), Complex Adaptive Systems Laboratory, University College Dublin, Dublin 4, Ireland

ARTICLE INFO

Article history:

Received 24 March 2015

Received in revised form 11 July 2015

Accepted 16 July 2015

Available online 5 August 2015

Editor: H. Stoll

Keywords:

salt marsh

foraminifera

Gulf Stream

Atlantic Ocean

late Holocene

ABSTRACT

We produced a relative sea-level (RSL) reconstruction from Connecticut (USA) spanning the last ~2200 yrs that is free from the influence of sediment compaction. The reconstruction used a suite of vertically- and laterally-ordered sediment samples ≤ 2 cm above bedrock that were collected by excavating a trench along an evenly-sloped bedrock surface. Paleomorph elevation was reconstructed using a regional-scale transfer function trained on the modern distribution of foraminifera on Long Island Sound salt marshes and supported by bulk-sediment $\delta^{13}\text{C}$ measurements. The history of sediment accumulation was estimated using an age-elevation model constrained by radiocarbon dates and recognition of pollution horizons of known age. The RSL reconstruction was combined with regional tide-gauge measurements spanning the last ~150 yrs before being quantitatively analyzed using an error-in-variables integrated Gaussian process model to identify sea-level trends with formal and appropriate treatment of uncertainty and the temporal distribution of data. RSL rise was stable (~1 mm/yr) from ~200 BCE to ~1000 CE, slowed to a minimum rate of rise (0.41 mm/yr) at ~1400 CE, and then accelerated continuously to reach a current rate of 3.2 mm/yr, which is the fastest, century-scale rate of the last 2200 yrs. Change point analysis identified that modern rates of rise in Connecticut began at 1850–1886 CE. This timing is synchronous with changes recorded at other sites on the U.S. Atlantic coast and is likely the local expression of a global sea-level change. Earlier sea-level trends show coherence north of Cape Hatteras that are contrasted with southern sites. This pattern may represent centennial-scale variability in the position and/or strength of the Gulf Stream. Comparison of the new record to three existing and reanalyzed RSL reconstructions from the same site developed using sediment cores indicates that compaction is unlikely to significantly distort RSL reconstructions produced from shallow (~2–3 m thick) sequences of salt-marsh peat.

© 2015 Elsevier B.V. All rights reserved.

1. Introduction

Common Era relative sea-level (RSL) reconstructions characterize natural variability, provide a long-term perspective against which to compare recent trends, and capture multiple phases of climate and sea-level behavior for model calibration. Along the

U.S. Atlantic coast, these reconstructions are primarily produced from cores of salt-marsh sediment and demonstrate that sea level departed positively and negatively from a stable mean, most noticeably since the onset of historic rates of rise (e.g. Kemp et al., 2011).

In high salt-marsh ecosystems on the U.S. Atlantic coast, RSL rise creates accommodation space that is filled by *in-situ* accumulation of peat. Through this response, salt-marshes preserve their elevation in the tidal frame and the salt-marsh surface tracks rising RSL (e.g. Bloom, 1964; Redfield and Rubin, 1962). Conse-

* Corresponding author. Tel.: +1 617 627 0869.

E-mail address: andrew.kemp@tufts.edu (A.C. Kemp).

quently, sequences of high salt-marsh peat are valuable archives from which RSL is reconstructed using proxies for tidal elevation (termed sea-level indicators) and a dated history of sediment accumulation. Foraminifera and plants are sea-level indicators because their distribution on modern salt marshes reflects the varied preferences and tolerances of species to inundation, which is primarily a function of tidal elevation (e.g. Scott and Mediolli, 1978). Sequences of salt-marsh sediment are usually recovered as a single core that is processed to provide vertically-ordered samples for reconstructing the tidal elevation at which each sample was originally deposited (termed paleomorph elevation, PME). A limitation of this approach is that thickening of the sequence as sediment accumulates may cause compaction of underlying material and post-depositional lowering of samples, resulting in an overestimation of the amount and rate of RSL rise (Bloom, 1964; Brain et al., 2012). RSL can also be reconstructed from discrete basal samples that minimize the influence of compaction, but do not provide a continuous record of Common Era RSL change (e.g. Redfield and Rubin, 1962). In Connecticut (and similar regions) it is possible to produce a continuous and basal RSL reconstruction using salt-marsh sediment that accumulated on top of incompressible bedrock or glacial erratics. Ice retreat from the modern Connecticut coast by ~18,000 yrs before present (Balco et al., 2009) exposed bedrock that was later transgressed by salt-marshes because Common Era RSL rose due to ongoing glacio-isostatic adjustment (GIA; e.g. Engelhart et al., 2011). The salt-marsh sediment deposited in contact with bedrock did not experience post-depositional lowering and preserves a compaction-free history of RSL change (Donnelly et al., 2004; Nydick et al., 1995).

We reconstruct RSL change during the last ~2200 yrs in Connecticut from salt-marsh sediment in direct contact with bedrock to answer two questions: (i) did persistent sea-level trends occur in Connecticut during the Common Era? and (ii) does sediment compaction materially alter patterns of RSL change reconstructed from cores of salt-marsh sediment? Samples from the sediment-bedrock contact were recovered by excavating a trench along the downward slope of a granite outcrop. Foraminifera and bulk sediment $\delta^{13}\text{C}$ values were used as sea-level indicators and sediment accumulation was dated using radiocarbon and regional pollution markers. The resulting RSL record was combined with instrumental measurements to identify positive and negative Common Era sea-level trends in Connecticut. Comparison with other RSL reconstructions from East River Marsh (Nydick et al., 1995) indicates that stratigraphies with intercalated peats are susceptible to compaction, but this compaction does not materially distort reconstructed RSL trends.

2. Study site

East River Marsh (Fig. 1) is typical of salt marshes in the northeastern United States (e.g. van de Plassche, 1991). Low-salt marsh environments are vegetated by *Spartina alterniflora* (tall form) and characterized by muddy sediment. This laterally-narrow floral zone exists between mean tide level (MTL) and mean high water (MHW). The high salt-marsh platform is found between MHW and mean higher high water (MHHW). It is vegetated by a mixed meadow of the C_4 plants *Spartina patens*, *Distichlis spicata*, and *Spartina alterniflora* (short form) and comprises most of the salt marsh by area. The transition between salt-marsh and freshwater ecosystems occurs between MHHW and highest astronomical tide (HAT). This zone is vegetated by the C_3 plants *Phragmites australis* and *Iva frutescens* at East River Marsh, but may also be characterized by sedges (e.g. *Schoenoplectus americanus*). The great diurnal tidal range at the site (mean lower low water, MLLW to MHHW) was estimated as 1.73 m using the NOAA vertical datum transformation tool for coastal regions (VDatum), compared

to 1.74 m measured by the NOAA tide gauge in Guilford Harbor (~1.5 km away; Fig. 1b).

3. Materials and methods

3.1. Site selection and trench sampling

East River Marsh was selected because granite bedrock outcrops above the salt-marsh surface and salt-marsh sediment is in direct contact with bedrock. We selected a location where the bedrock sloped evenly at ~30° to a depth of ~2.4 m below the modern marsh surface (Fig. 2a). Assuming that GIA caused ~1.0 mm/yr of Common Era RSL rise in southern Connecticut (e.g. Donnelly et al., 2004; Engelhart et al., 2009; Peltier, 1996), we anticipated that the selected location would provide a continuous sequence of compaction-free sediment spanning the entire Common Era. A trench was excavated to expose the bedrock-sediment contact (Fig. 2). The basal sediment was segmented at slight changes in bedrock slope and recovered as a series of adjacent blocks. Sample elevations were measured by leveling the four corners of each block in contact with bedrock to a temporary benchmark, the elevation of which was established (relative to NAVD88) by real time kinematic satellite navigation. Each block was wrapped in plastic, labeled to preserve its original orientation, and refrigerated. The blocks were subsequently cut into 1-cm thick basal samples representing 1-cm increments of elevation (Fig. 2b). This approach created a suite of vertically- and laterally-ordered sediment samples that were deposited ≤ 2 cm above the bedrock surface. The position of each sampled is expressed in a two-dimensional (depth and distance) co-ordinate system where the top of the trench (1.01 m above MTL) is the origin. Sample positions discussed in the text and presented on figures use this reference frame. All subsequent analyses (radiocarbon and pollution dating, foraminiferal counts, and $\delta^{13}\text{C}$ measurements) were performed on this set of samples that we consider to be free from the effects of sediment compaction. In most cases a thin (<2 mm) mat of fine roots was removed from the bottom of each sample and discarded after inspection. This mat formed by the growth of roots from younger plants at the surface along the sediment-bedrock interface.

3.2. Modern foraminifera

At 12 salt marshes we established transects across the prevailing elevation and environmental gradient to describe the modern distribution of foraminifera (Fig. 1a). These sites represent the spatial, ecological, and geomorphological range of salt marshes on the north coast of Long Island Sound and complement the distribution of existing modern datasets. At East River Marsh we sampled two parallel transects (Fig. 1c) that included highest-marsh environments where the shallow, amorphous sediment overlying bedrock is analogous to the basal sediment that accumulated in the trench. Similar highest salt-marsh sediments and environments were also sampled at other sites. We combined the new dataset of modern foraminifera with those summarized by Wright et al. (2011) to produce a regional training set consisting of 254 modern foraminifera samples from 16 sites on the north coast of Long Island Sound (Fig. 1) including 92 samples from four Connecticut sites that were reported in published literature (Edwards et al., 2004; Gehrels and van de Plassche, 1999). The new modern foraminifera data are presented in the supporting appendix.

3.3. Reconstructing paleomorph elevation

A weighted-averaging transfer function with inverse deshrinking (WA-inv) was developed to quantify the relationship between

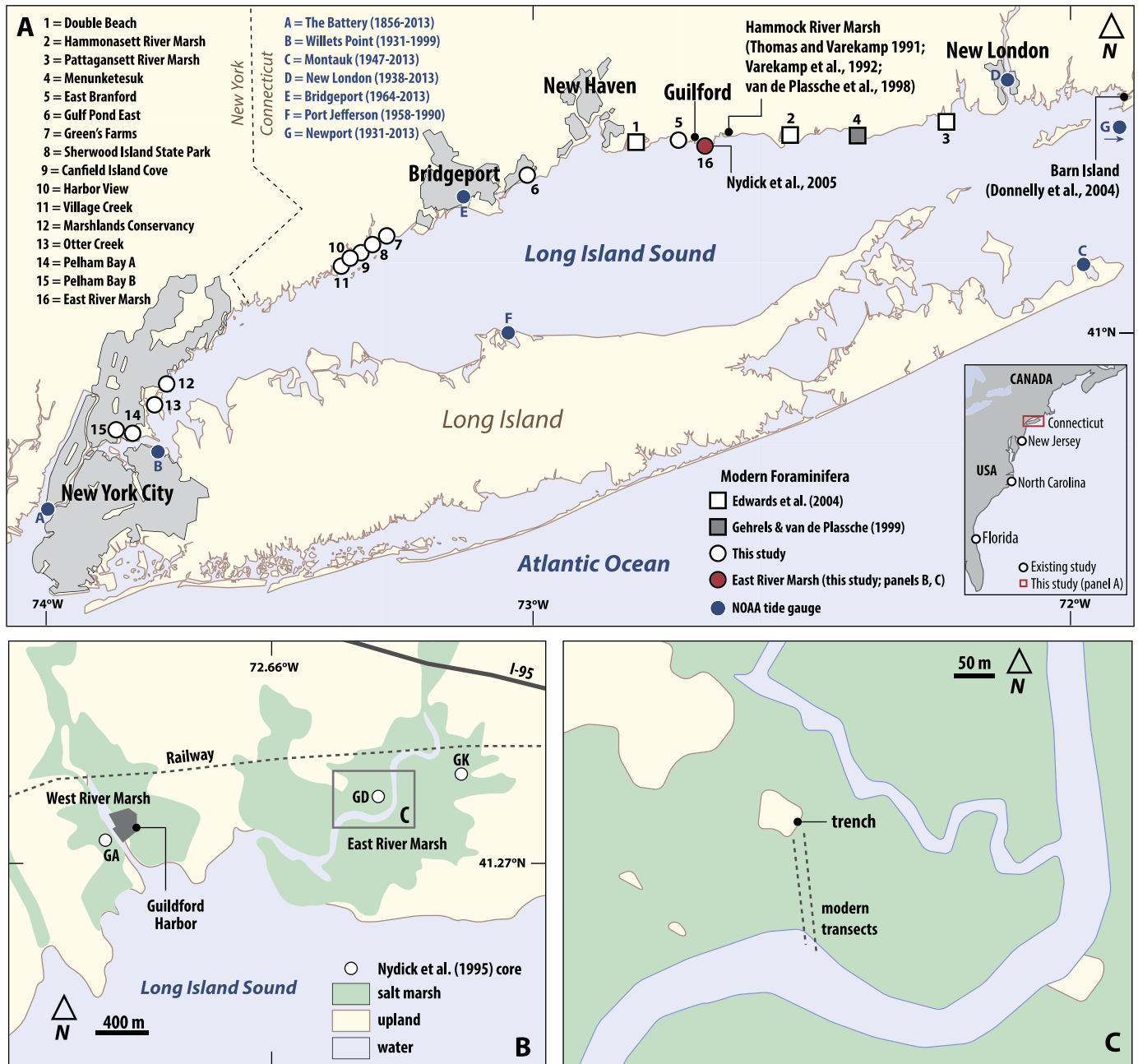


Fig. 1. (A) Location of East River Marsh (red circle) on the Long Island Sound coast of Connecticut. Transects of modern (surface) foraminifera were collected from 12 new sites including East River Marsh (# 5–16) and combined with published datasets (# 1–4) to generate a training set of 254 samples. NOAA tide-gauge locations are represented by labeled (A–E) blue circles. Inset shows the location of other high-resolution reconstructions of Common Era sea level from the U.S. Atlantic coast. (B, C) Location of the trench and modern transects sampled at East River Marsh. The approximate location of three cores used to reconstruct relative sea level by Nydick et al. (1995) are represented by open circles and labeled using the abbreviations provided in the original publication. (For interpretation of the references to color in this figure legend, the reader is referred to the web version of this article.)

modern foraminifera and tidal elevation from the expanded modern dataset. Model comparisons are presented and discussed in the Supporting Material. To combine data from sites with different tidal ranges into a regional training set, we applied a standardized water level index (e.g. Horton, 1999).

$$SWLI = \frac{Alt_{ab}}{MHHW_b - MTL_b} * 100$$

where Alt_{ab} is the measured altitude of sample a collected at site b (expressed relative to MTL) and $MHHW_b - MTL_b$ are tidal datums at site b . The highest occurrence of foraminifera (Wright et al., 2011) was not used as a SWLI datum because at some sites

foraminifera were present in all surface samples meaning that their highest occurrence was not captured. The WA-inv transfer function was applied to the trench samples from which foraminifera were enumerated to reconstruct PME. A sample-specific ($\sim 1\sigma$) uncertainty (Juggins and Birks, 2012) was calculated for each PME estimate by bootstrapping ($n = 1000$). Transfer function output was in SWLI units and converted to MTL using the modern tidal prism at East River Marsh. The ecological plausibility of PME reconstructions was judged by measuring the dissimilarity between trench samples and their closest analogue in the modern training set using the Bray–Curtis distance metric. If the distance exceeded the 20th percentile of distance calculated among all pairings of

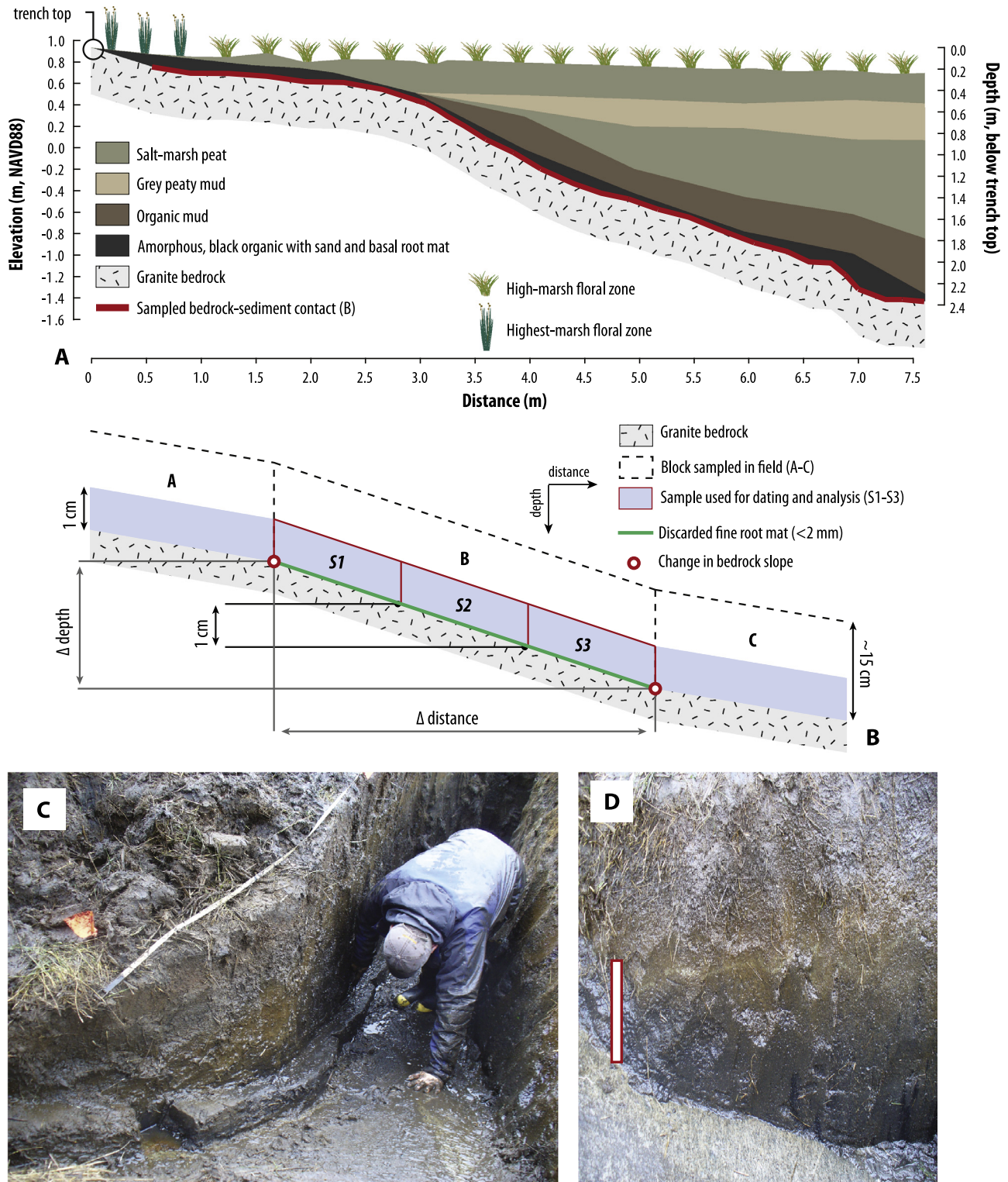


Fig. 2. (A) Profile of the trench excavated at East River Marsh. The bedrock-sediment contact (red line) was sampled and used to reconstruct relative sea level. The high salt-marsh floral zone is vegetated by *Distichlis spicata* and *Spartina patens*. The highest salt-marsh floral zone is vegetated by *Iva frutescens* and *Phragmites australis*. NAVD88 = North American Vertical Datum of 1988. (B) Schematic of trench sampling (not drawn to scale). In the field, the trench profile was segmented into blocks (A–C) at changes in bedrock slope. All blocks were positioned in a co-ordinate system of depth and distance by surveying the four bottom corners that were in contact with the bedrock. The origin for this co-ordinate system was the trench top (panel A). The blocks (with a height of ~15 cm) were sampled, wrapped in plastic with their orientation labeled and returned to the laboratory for sub-sampling. Individual blocks were cut into sub samples (S1–S3) that each represented a depth change (Δ depth) of 1 cm by assuming that the measured slope of the bedrock (Δ distance/ Δ depth) was constant for each block. Sample thickness was 1 cm and a mat of fine roots (<2 mm thick) was removed from the bottom of the samples where necessary and discarded following inspection. All analysis (radiocarbon and pollution dating, $\delta^{13}\text{C}$ measurements, and counts of foraminifera) was conducted on samples produced using this approach. All samples were from the unit of amorphous, black organic with sand unit. (C) Photograph of sampling sediment blocks in the field by cutting the trench wall to leave an over-sized step that was segmented into blocks at changes in bedrock slope. (D) Photograph from the excavated trench showing the contact between the granitic bedrock and overlying accumulation of salt-marsh sediment. The black amorphous organic unit is overlain by brown organic mud. The height of the white scale bar is approximately 5 cm. (For interpretation of the references to color in this figure legend, the reader is referred to the web version of this article.)

Table 1
Radiocarbon ages from the East River Marsh trench.

Elevation (cm below trench top)	ID	^{14}C Age	^{14}C Age Error	$\delta^{13}\text{C}$ (‰, VPDB)	Description
56	OS-88674	175	30	−15.20	<i>Distichlis spicata</i> rhizome
66	OS-86561	345	25	−13.25	<i>Distichlis spicata</i> rhizome
78	OS-86562	550	30	−12.81	<i>Distichlis spicata</i> rhizome
90	OS-89141	835	25	−14.52	<i>Distichlis spicata</i> rhizome
111	OS-86567	1080	30	−26.59	Unidentified woody rhizome
146	OS-86616	1300	25	−16.23	<i>Distichlis spicata</i> rhizome
156	OS-86560	1490	25	−13.28	<i>Distichlis spicata</i> rhizome
158	OS-89764	1490	30	−14.56	<i>Distichlis spicata</i> rhizome and bulb
165	OS-89059	1570	25	−14.03	<i>Distichlis spicata</i> rhizome
184	OS-88962	1790	25	−24.89	Piece of wood
195	OS-86563	1830	30	−26.33	Unidentified woody rhizome
207	OS-88656	1940	30	−23.26	Piece of wood
214	OS-86550	2050	25	−24.31	Unidentified woody rhizome
224	OS-88615	2050	45	−26.03	Piece of wood
231	OS-88616	2080	40	−24.36	Piece of wood

Radiocarbon ages reported by the National Ocean Sciences Accelerator Mass Spectrometry facility for samples in the East River Marsh trench. Reported $\delta^{13}\text{C}$ values are from an aliquot of CO_2 collected during sample combustion.

modern samples, the trench sample was classified as lacking a modern analogue and was excluded from the RSL reconstruction.

3.4. $\delta^{13}\text{C}$ measurement

In the northeastern U.S. and maritime Canada, *in-situ* deposition of plant material is the primary source of salt-marsh organic material (e.g. Chmura and Aharon, 1995). Therefore the ratio of stable carbon isotopes ($\delta^{13}\text{C}$) in bulk sediment reflects the dominant vegetation community at the time of deposition (e.g. Middleburg et al., 1997) and can be used as a sea-level indicator if the plant community has a systematic relationship to tidal elevations (Johnson et al., 2007; Kemp et al., 2013a). Bulk sediment $\delta^{13}\text{C}$ values were measured using the methods and instruments described in Kemp et al. (2013a).

3.5. Trench chronology

The timing of basal sediment deposition was constrained by radiocarbon dating of plant macrofossils in growth position and small pieces of wood that we interpreted as having been deposited on a paleo-marsh surface (Table 1). After separation from the sediment matrix, 15 radiocarbon samples were cleaned under a microscope to remove in-growing younger roots and older adhered sediment, oven dried (45 °C), and submitted to National Ocean Science Accelerator Mass Spectrometry (NOSAMS) facility for dating. All samples underwent standard acid-base-acid pretreatment at NOSAMS.

Recognition of pollution horizons of known age from trends in concentrations of copper, lead, mercury, ^{137}Cs , and ratios of stable lead isotopes (^{206}Pb : ^{207}Pb) established the timing of recent sediment deposition, because the utility of radiocarbon for material younger than ~350 yrs is hindered by a plateau in the calibration curve. Copper, lead, and ^{206}Pb : ^{207}Pb trends and their stratigraphic position were matched to features of historic production and consumption, which were assumed to approximate the timing and relative magnitude of atmospheric emissions and deposition (Gobeil et al., 2013; Kemp et al., 2012a; Lima et al., 2005). Trends in mercury concentration were matched to those reported at nearby sites in cores of independently dated salt-marsh sediment (e.g. Varekamp et al., 2003). Peak ^{137}Cs activity was assigned an age of 1963 CE reflecting the peak in above ground testing of nuclear weapons. Elemental concentrations and Pb isotopes were measured using the methods and instruments

described in Vane et al. (2011) and Kemp et al. (2012a). Mercury measurements were made on a Milestone DMA-80 direct mercury analyzer at Yale University. Activity of ^{137}Cs was measured by gamma spectroscopy at Yale University using standard methods.

All age estimates were assimilated into a single age-elevation model using Bchron, which produces posterior estimates of sample age using Markov Chain Monte Carlo simulation, each of which is equi-probable (Haslett and Parnell, 2008; Parnell et al., 2008). The resulting suite of chronologies is summarized by Bchron to estimate sample ages with a 95% uncertainty interval. Radiocarbon ages were specified as having a thickness of 2 cm to recognize that plant macrofossils grow slightly below the surface on which contemporary foraminifera lived. This approach acknowledges uncertainty in contrast to adjusting the depths of radiocarbon dates by a fixed amount. Chrono horizons established from ^{137}Cs and pollution markers were treated as having uniform probability distributions.

3.6. Relative sea-level trends

RSL was reconstructed by subtracting PME from measured sample elevation, where both quantities were expressed relative to MTL. When combined with age estimates from the age-elevation model, the RSL reconstruction is characterized by data points that are unevenly distributed through time and have a unique combination of vertical and temporal uncertainty. The RSL reconstruction was combined with a regional tide-gauge record from Long Island Sound. Annual tide-gauge measurements from The Battery, Willets Point, Port Jefferson, Bridgeport, New London, Montauk, and Newport (Fig. 1a) were averaged to produce a single instrumental RSL record with a vertical uncertainty estimated by calculating the annual standard deviation across six of the tide gauges for 1950–2013 CE (the Port Jefferson gauge ceased recording in 1990 CE and therefore was not included in this estimate of uncertainty). The average of these annual standard deviations was 0.011 m and an uncertainty of ± 0.022 m was applied to each annual data point along with an age uncertainty of ± 0.5 yrs.

Quantitative RSL trends with formal uncertainties were estimated by applying an error-in-variables integrated Gaussian process (EIV-IGP) model (Cahill et al., 2015) to the combined RSL dataset of proxy reconstructions and tide-gauge measurements. The EIV component (Dey et al., 2000) accounts for error in the explanatory variable (sample age), which is assumed to be fixed and known in standard regression. Since sample ages are uncertain, the EIV approach is appropriate and necessary. The Gaussian

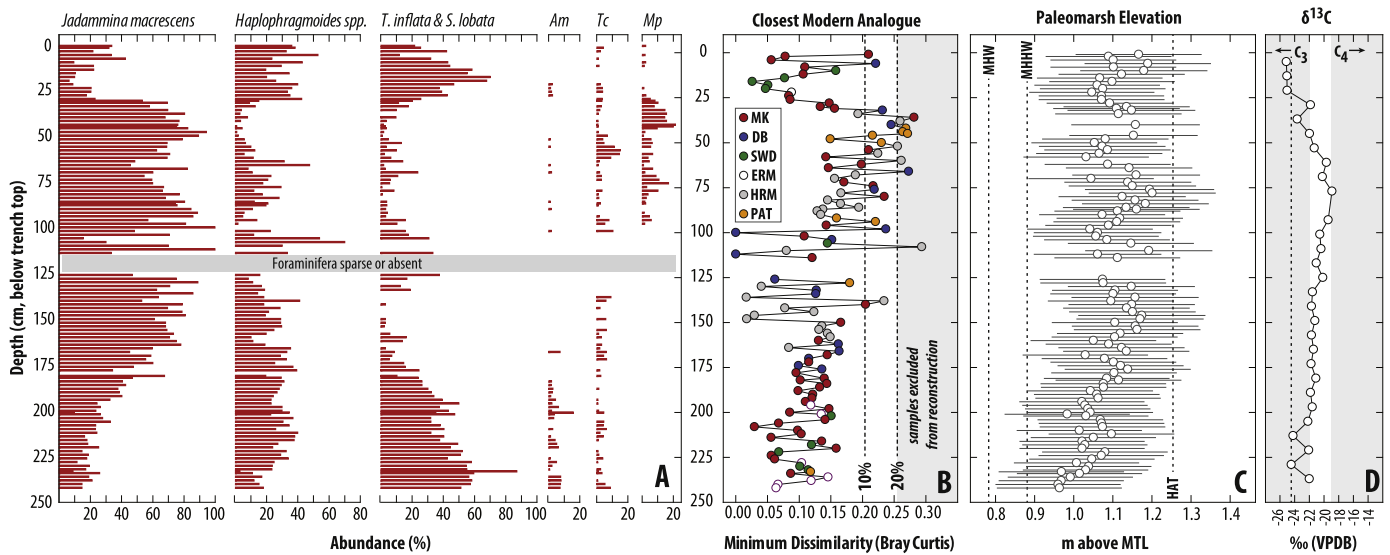


Fig. 3. (A) Relative abundance of the six most common species of foraminifera from samples in the East River Marsh trench. Am = *Arenoparrella mexicana*, Tc = *Tiphrotrachna comprimata*, Mp = *Miliammina petila*. (B) Dissimilarity between trench samples and their closest analogue in the modern training set measured using the Bray–Curtis distance metric. Symbol colors denote the site where the closest analogue was located. DB = Double Beach, ERM = East River Marsh, HM = Hammonasset River Marsh, MK = Meunketesuk, PAT = Pottagansett River Marsh, SWD = Sherwood Island State Park. Samples exceeding the 20th percentile of dissimilarity measured in modern samples were deemed to lack an adequate modern analogue and were excluded from the reconstruction. Circles represent mid points and error bars are the sample-specific uncertainty estimated by bootstrapping. Vertical dashed lines mark the elevation of mean high water (MHW), mean higher high water (MHHW), and highest astronomical tide (HAT). (C) Paleomarch elevation (PME) reconstructed using the weighted averaging transfer function. Circles represent mid points and error bars are the sample-specific uncertainty estimated by bootstrapping. Vertical dashed lines mark the elevation of mean high water (MHW), mean higher high water (MHHW), and highest astronomical tide (HAT). (D) Measured $\delta^{13}\text{C}$ values from samples of bulk trench sediment. Left shaded area denotes samples more depleted than -22‰ that are typical of salt-marsh environments above MHHW in mid-Atlantic and New England salt marshes, Right area denotes samples less depleted than -18.9‰ that are typical of salt-marsh environments below MHHW in mid-Atlantic and New England salt marshes. The dashed vertical line at -24.5‰ is the reported value for bulk sediment sample from a salt-marsh to upland transition in the Great Marshes of Massachusetts (Middleburg et al., 1997).

process component (Rasmussen and Williams, 2005) is a practical approach to modeling non-linear time series data such as RSL reconstructions. We model the rate of sea-level change (i.e. the first derivative) and subsequently integrate it to form an integrated Gaussian process (IGP; Holsclaw et al., 2013), which aims to match RSL. The Gaussian process has a prior distribution specified by a mean function (here set to a constant) and a covariance function that determines the smoothness of the reconstructions. In this Bayesian model, the posterior rate and covariance function are learnt from the data. The IGP component is embedded within the EIV framework to account for age uncertainties, vertical uncertainties, and the covariance that is introduced by removing a rate of GIA. The model does not account for uncertainty in the rate of GIA, which must be specified as an input.

The covariance function of the Gaussian process prior placed on the rate of sea-level is structured such that the correlation between two individual data points depends on the time difference between them rather than their absolute position in time. For example, it assumes that the magnitude of the change in rate between two data points at 1880 CE and 1890 CE will be approximately the same as two data points at 1980 CE and 1990 CE. Whilst the integrated process (representing sea level itself) can display more complex behavior, previous work showed that this global smoothness assumption is robust to mis-specification (Cahill et al., 2015), especially once we account for the uncertainties in both age and elevation. This approach captures the continuous and dynamic evolution of RSL change with full consideration of many sources of uncertainty. Modeled uncertainties are smaller than those of the original reconstruction because the EIV-IGP model exploits the probability distribution (vertical and temporal) within a single data point and the relationship among temporally-ordered data points to produce probabilistic estimates of sea level and the rate of sea-level change at any point in time. We also used change point analysis to provide a best estimate of when modern rates of sea-level rise began following the approach described in Kemp et al. (2013a).

4. Results

4.1. Trench stratigraphy, foraminifera, and $\delta^{13}\text{C}$

The excavated trench was ~ 8 m long and reached a maximum depth of ~ 2.4 m. The basal sediment (approximately 3–20 cm thick) in contact with bedrock was uniformly a black, amorphous organic unit with angular, sand-sized grains eroded from the underlying granite and sparse plant macrofossils (Fig. 2). This unit is analogous to surface sediment from the margin between highest salt-marsh environments and bedrock islands at East River Marsh, including the upper reaches of the sampled trench. The overlying sediment exposed in the trench included salt-marsh peat with abundant, *in-situ* remains of *Distichlis spicata* and *Spartina patens*, as well as a grey, peaty-mud unit.

Foraminifera were enumerated from 121 evenly-spaced trench samples to reconstruct PME (Fig. 3a). From 242 cm to 178 cm below the trench top, the most common species of foraminifera were *Trochammina inflata* and *Siphotrochammina lobata* (average 45% of individuals). From 176 cm to 31 cm, *Jadammina macrescens* was the most abundant species (average 65% of individuals). The uppermost 30 cm was characterized by increased abundances of *Haplophragmoides* spp. (average 34% of individuals) with *Trochammina inflata* and *Siphotrochammina lobata* (average 41% of individuals). Between 108 cm and 124 cm foraminifera were sparse (< 5 individuals) or absent. Intervals of low test abundance could be the result of test dissolution or low concentrations of tests as a consequence of low reproduction rates, high sedimentation rates, or patchy distributions.

To identify samples lacking a modern analogue, dissimilarity between populations of foraminifera preserved in trench samples and their modern counterparts was measured using the Bray–Curtis metric (Fig. 3b). The closest modern analogues for trench samples were drawn from six different sites, which likely reflects sub-regional spatial variability in the composition of high-marsh assemblages as observed on modern salt marshes in Connecti-

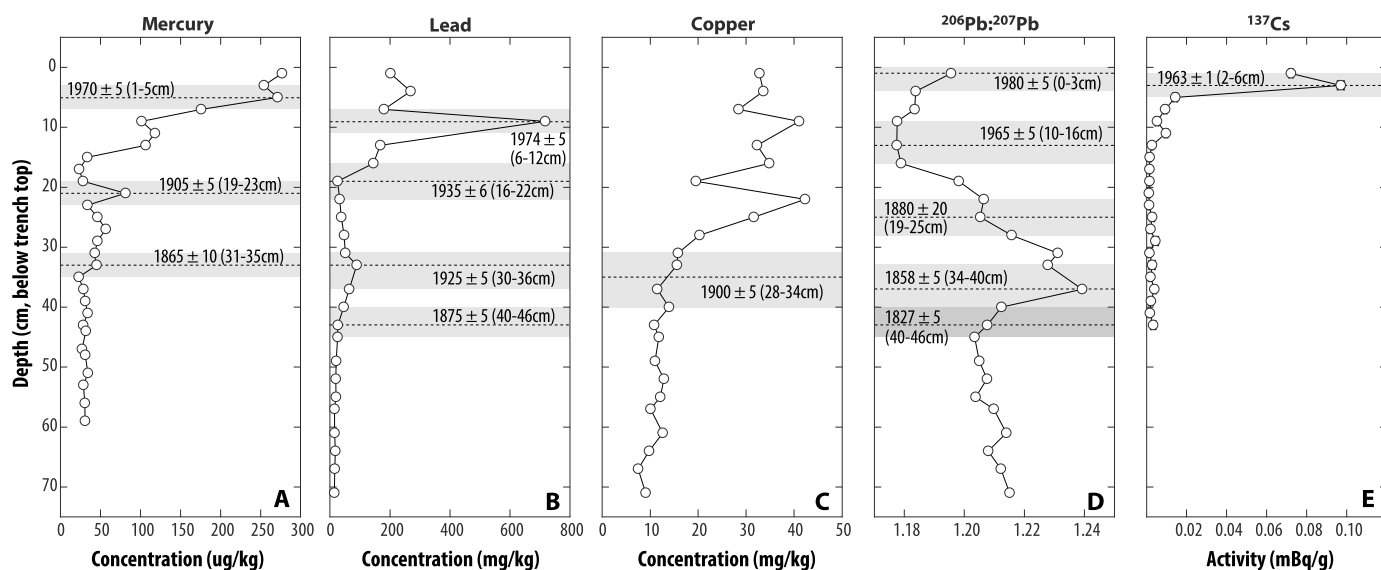


Fig. 4. Down-core profiles of elemental abundances and isotopes used to recognize historical pollution markers. The age (year CE) and depth (with uncertainty) of each marker are listed and the grey shading denotes vertical uncertainty assigned to each chronohorizon for inclusion in the Bchron age-depth model. Analytical uncertainties are smaller than symbols used.

cut and elsewhere (e.g. Kemp et al., 2013b; Wright et al., 2011). The distance between nine trench samples and their closest modern analogue exceeded the 20th percentile of dissimilarity measured among all pairings of modern samples and these samples were excluded from further analysis. Eight of the excluded samples (36–66 cm) were characterized by high abundances of *Jadammina macrescens* (>68%) and the presence of *Miliammina petila* (4–21%; average 14%). The modern training set includes samples with comparable abundances of *Jadammina macrescens* (up to 100%) and *Miliammina petila* (up to 10%, excluding a single sample of 63% from East River Marsh). However, the maximum abundance of *Jadammina macrescens* in modern samples containing at least 1% *Miliammina petila* was 34%. The unusual co-occurrence of these two species caused the trench samples to lack a modern analogue.

Application of the WA-inv transfer function to the remaining 112 samples produced PME reconstructions with sample-specific uncertainties that ranged from ± 0.158 m to ± 0.165 m, equivalent to approximately $\pm 10\%$ of great diurnal range at East River Marsh (Fig. 3c). These results show that the samples were deposited between MHHW and HAT at the leading edge of a RSL transgression and are supported by bulk sediment $\delta^{13}\text{C}$ values of -25.1‰ to -18.9‰ indicating significant input from C_3 vegetation (Fig. 3d). Along the U.S. mid-Atlantic and northeastern coasts, these $\delta^{13}\text{C}$ values coupled with the presence of agglutinated foraminifera demonstrate that the samples formed at or above MHHW, but below HAT or the highest occurrence of foraminifera (Johnson et al., 2007; Kemp et al., 2013a; Middleburg et al., 1997). The samples where foraminifera were sparse or absent probably formed in an environment between MHW and HAT (Engelhart et al., 2011; van de Plassche, 1991) as evidenced by $\delta^{13}\text{C}$ values between those typical of C_3 and C_4 plants (coupled with sediment texture that is the same throughout the basal section of the trench). Measured $\delta^{13}\text{C}$ values were not used to constrain PME reconstructions because most samples had values between those of C_3 and C_4 vegetation. When salt-marsh sediment is sampled with a core, the location of the PME reconstruction is static and the change from highest salt-marsh peat to high salt-marsh peat that occurs because of RSL rise happens only once. Deeper samples in the core have $\delta^{13}\text{C}$ values that are typical of the C_3 plants that occupy elevations above MHHW. Samples further up the core have $\delta^{13}\text{C}$ values that are typical of the C_3 plants that occupy elevations be-

low MHHW (see for example Kemp et al., 2012b). In contrast, the sediment used in the trench reconstruction tracks the lateral and vertical RSL transgression, which is reflected in the bulk sediment samples having intermediate $\delta^{13}\text{C}$ values because all of the samples were likely deposited close to MHHW. Therefore it was not possible to use $\delta^{13}\text{C}$ values to reduce reconstruction error as they were elsewhere (Kemp et al., 2013a).

4.2. Trench chronology

Fifteen radiocarbon dates demonstrate that the trench spans the interval since ~ 200 BCE (Table 1). The uppermost part of the core was dated by identifying pollution chronohorizons that were related to historic events such as above-ground testing of nuclear weapons and trends in national and regional (Upper Mississippi Valley) industrial production (Fig. 4). We assumed that industrial emissions were transported to East River Marsh by prevailing wind patterns and deposited on the salt-marsh surface within a few years and without further isotopic fractionation (e.g. Gobeil et al., 2013). Trends rather than absolute values were the basis for recognizing chronohorizons because emissions rates per unit of production changed through time. The accuracy of this approach in eastern North America was demonstrated in studies that validated chronologies established from pollution markers against independent age constraints such as ^{210}Pb in salt-marsh sediment (Gobeil et al., 2013; Kemp et al., 2012a) and varved lake sediments (Lima et al., 2005). Discrepancies among sample ages estimated from different pollution markers (Fig. 4) may arise due to local-scale variability in the trends and timing of pollution or from chemical mobility in the sediment profile. Bchron produces probabilistic age estimates and negates the need to choose among conflicting pollution markers by identifying chronologies that are more and less likely to be accurate rather than discarding outliers. The Bchron age-elevation model estimated the age of each trench sample with an average 95% credible interval of approximately ± 50 yrs (Fig. 5). In the upper part of the core, this credible interval overlaps with the individual uncertainties of 12 of the 14 pollution markers.

4.3. Relative sea-level change

Annual tide-gauge measurements from seven locations in and near Long Island Sound (Fig. 1) are highly correlated, indicating

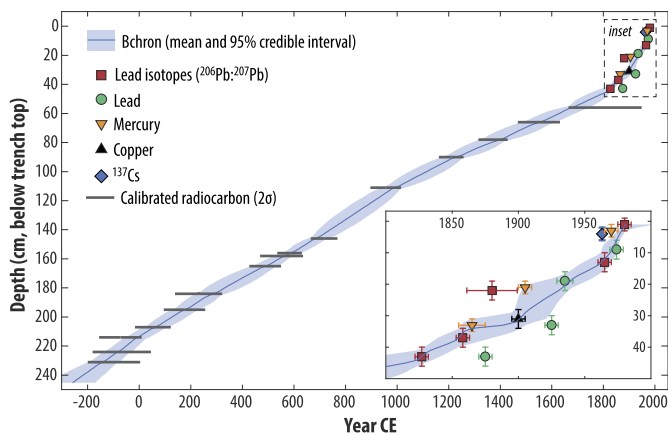


Fig. 5. Age-depth model developed for the East River Marsh trench. The shaded blue envelope is the 95% credible interval. Calibrated radiocarbon ages are the 2σ range between the youngest and oldest possible ages and do not represent the probability distribution associated with ages within the range. Inset shows detailed chronology for the last ~ 200 yrs. (For interpretation of the references to color in this figure legend, the reader is referred to the web version of this article.)

that the long-term trends and decadal variability they recorded were regional in scale and justifying the creation of an averaged record (although The Battery was the only instrument in operation for the period between 1856 CE and 1930 CE; Fig. 6a). The East River Marsh RSL reconstruction is comprised of 112 datapoints, each of which has a unique combination of vertical and temporal uncertainty (Fig. 6b); data provided in supporting appendix). The averaged tide-gauge record lies within the uncertainty of the reconstruction and the two datasets were combined prior to analysis. Application of the EIV-IGP model (Fig. 6c) shows that RSL rose at ~ 1 mm/yr from ~ 200 BCE to ~ 1000 CE. The rate of RSL rise subsequently decelerated to a minimum of 0.41 mm/yr (0.17–0.63 mm/yr; 95% credible interval) at ~ 1400 CE. The 95% credible interval of the model predictions at ~ 1600 – 1800 CE lie below the mid-point of RSL reconstructions, but within their uncertainty (Fig. 6c). RSL rise then accelerated continuously to a current rate of 3.2 mm/yr (2.93–3.49 mm/yr; 95% credible interval), which is the fastest rate of century-scale rise in at least the last 2200 yrs (Fig. 6d). Change-point analysis performed on the combined proxy and instrumental dataset showed a significant increase in the rate of RSL rise at 1850–1886 CE (95% credible interval).

5. Discussion

5.1. Relative sea-level change and sediment compaction at East River Marsh

Previous research in Connecticut established the framework for producing continuous RSL reconstructions using single cores of salt-marsh sediment (e.g. Thomas and Varekamp, 1991; van de Plassche et al., 1998; Varekamp et al., 1992). RSL change during the last ~ 1500 yrs at East River Marsh and West River Marsh was reconstructed by Nydick et al. (1995) using three cores of high salt-marsh sediment (GA, GD, and GK; Fig. 1). Each core was dated using five radiocarbon ages and by identifying the onset of anthropogenic pollution (1877 CE ± 15 yrs) from down-core copper and zinc concentrations. We investigated the influence of compaction on sequences of salt-marsh sediment by comparing the compaction-free RSL reconstruction from the trench to those generated from cores. We assumed that any differences among the four RSL reconstructions were principally the result of sediment compaction because other local factors such as tidal-range change should be consistent among records in such close proximity to one

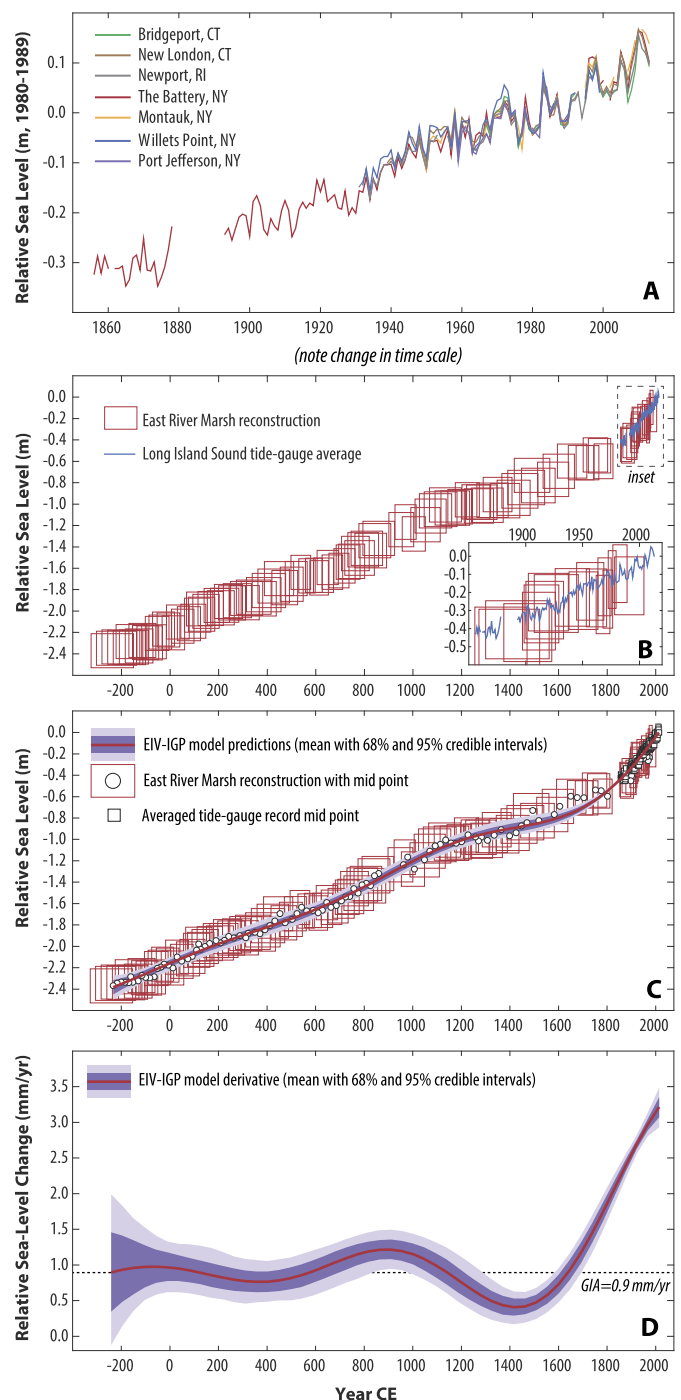


Fig. 6. (A) Annual tide-gauge measurements from seven locations in Long Island Sound expressed relative to the 1980–1989 CE average. This reference period was used because the Port Jefferson instrument ceased recording in 1990 CE. (B) Relative sea level reconstructed from the East River Marsh trench. Each box represents a single datapoint with vertical and temporal uncertainty from the transfer function and age-depth model respectively. The average tide-gauge record is expressed with respect to the 2013 CE average to ensure that it can be compared directly to the RSL reconstruction. (C) Errors-In-Variables Integrated Gaussian Process (EIV-IGP) fitted to the combined relative sea-level data from the East River Marsh proxy reconstruction and the Long Island Sound averaged tide-gauge record. (D) Rate of relative sea-level change estimated by the EIV-IGP model.

another. To ensure that all the reconstructions could be meaningfully compared, we reanalyzed cores GA, GD, and GK by applying our Long Island Sound transfer function to the reported assemblages of foraminifera and developing a Bchron age-depth model using the reported radiocarbon ages and position of the pollution

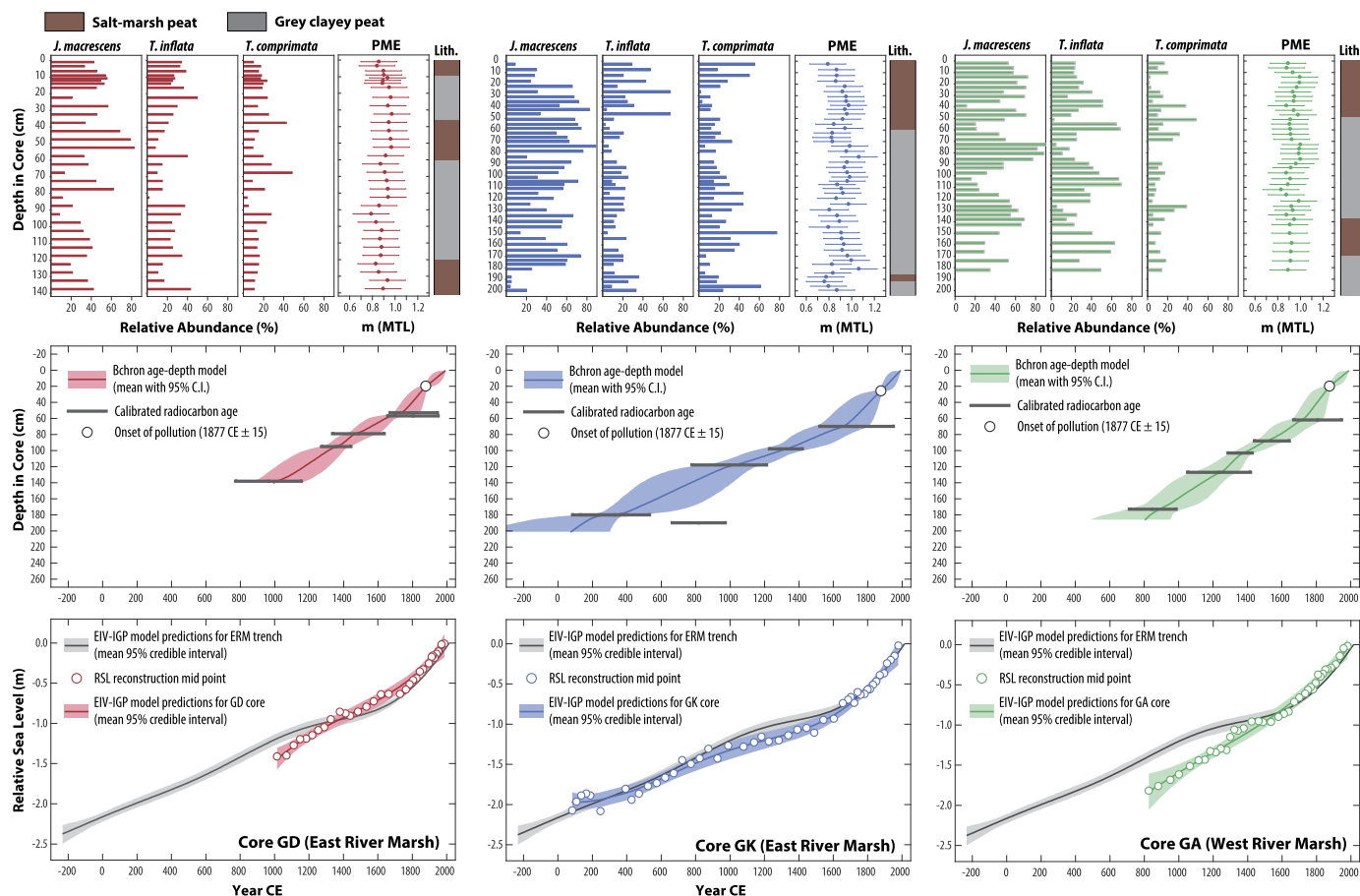


Fig. 7. Reanalysis of the three cores (GD, GK, and GA, distinguished by color) used by Nydick et al. (1995) to reconstruct relative sea level at East River Marsh and West River Marsh. The abundance of the three most common species of foraminifera reported by Nydick et al. (1995) are shown in the top row of panels. Application of the Long Island Sound transfer function to these assemblages reconstructed paleommarsh elevation (PME). Simplified core lithology is modified after Nydick et al. (1995). An age-depth model was generated for each core using the radiocarbon ages and pollution marker reported in the original study (middle row of panels). This reanalysis generated a relative sea level (RSL) reconstruction for each core (lower row of panels) that followed a similar approach to the reconstruction from the East River trench to allow direct and fair comparison among records. The reconstructions from each core were analyzed by the error-in-variables integrated Gaussian process (EIV-IGP) model. The trench reconstruction is also represented by results from the EIV-IGP model.

marker as input. We estimated core-top elevations using the transfer function reconstruction for the surface sample in each core. This reanalysis generated three RSL reconstructions to compare with the trench reconstruction (Fig. 7).

The RSL reconstruction from the trench lies within the uncertainty of the GK record indicating a lack of detectable compaction. In contrast, the trench reconstruction is above (and outside of) the uncertainty bounds of the GA reconstruction prior to ~1300 CE and is higher than the RSL reconstruction from GD prior to ~1200 CE. Cores GA and GD include units of salt-marsh peat that are intercalated by grey, clayey peat (Fig. 7). Empirical data (e.g. Bloom, 1964) and modeling studies (Brain et al., 2012) show that intercalated peat is susceptible to compaction. In contrast, continuous sequences of high salt-marsh peat (such as those used elsewhere along the U.S. Atlantic coast; Fig. 8) undergo little compaction (Brain et al., 2015). The pattern of increasing difference with depth and age between RSL reconstructed from the trench and cores GA and GD is suggestive of post-depositional lowering of the core samples and indicates that sediment compaction may distort RSL reconstructions generated from stratigraphies that include intercalated salt-marsh peats. This distortion is greatest (0.42 m) at ~830 CE in core GA, but with consideration of uncertainties in the EIV-IGP models it could range from 0.13 m to 0.72 m. However, there is no detectable compaction in core GK despite it being a longer-duration record produced from a sedimentary sequence that also includes intercalated peat. It is likely that the accuracy

of the lowest radiocarbon date in core GA rather than compaction is the primary reason for the difference to the trench reconstruction. These comparisons suggest that compaction did not materially distort the reconstructions and that single cores of salt-marsh sediment can be representative of the principal RSL trends that occurred at a site if placed in, and supported by, an appropriate stratigraphic and chronological framework.

5.2. Sea-level change on the U.S. Atlantic coast

During most of the Common Era, spatially-variable GIA was the primary driver of RSL change along the U.S. Atlantic coast. GIA includes a component of vertical land motion driven by the collapse of the Laurentide Ice Sheet's proglacial forebulge and also a geoid component resulting from the redistribution of mass as mantle material returns to regions beneath formerly glaciated areas. Predictions from Earth-ice models (e.g. Peltier, 1996) and RSL reconstructions (e.g. Engelhart et al., 2009) show that the rate of Common Era and ongoing GIA varies systematically with distance from the former center of the Laurentide Ice Sheet. The ICE6G-CVM5a model (Peltier et al., 2014) predicts a current GIA-driven RSL rise of ~1.0 mm/yr at East River Marsh. Similarly, at Barn Island, Connecticut (Fig. 1a), a compaction-free RSL reconstruction spanning the period ~1300–1850 CE estimated the background rate of Common Era RSL rise to be 1.0 ± 0.2 mm/yr (Donnelly et al., 2004). Under the assumption that RSL change over this period was driven

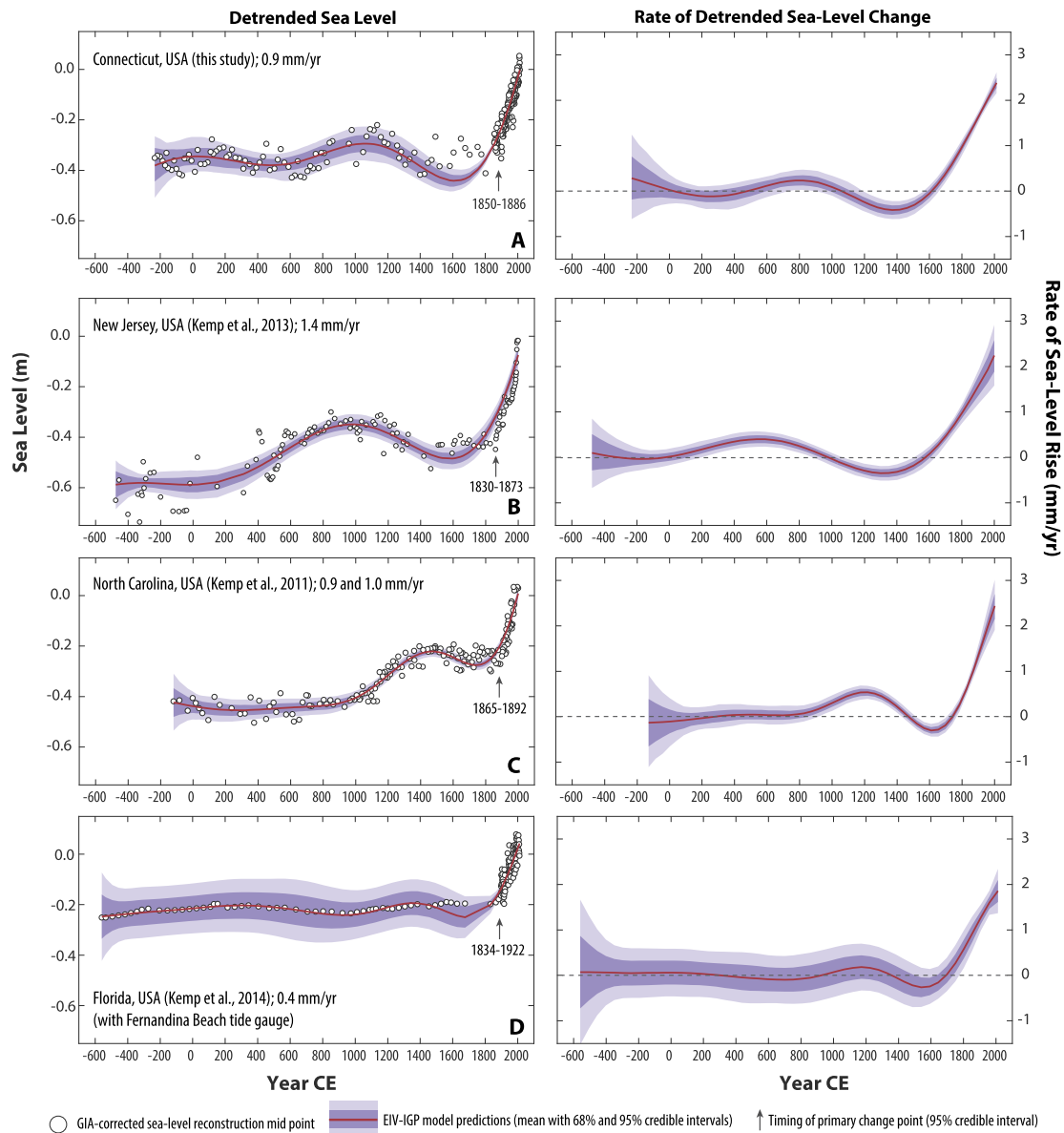


Fig. 8. Common Era sea-level change on the U.S. Atlantic coast. Reconstructions are organized by latitude from north (A) to south (D). Each reconstruction was analyzed using the Errors-In-Variables Integrated Gaussian Process (EIV-IGP) model to ensure fair comparison among records. Left-side panels are sea-level reconstructions after removing an estimated rate of glacio-isostatic adjustment (listed in panel title). Labeled arrows indicate the timing of the primary change in the rate of sea-level estimated using change point regression by applying the same model to all data sets. Right-side panels show estimated rates of sea-level change after detrending. Scales are standardized within each column of panels for comparability among records.

exclusively by GIA and any other process(es) causing vertical land motion (such as dynamic topography; e.g. Rowley et al., 2013), this rate is an estimate of the ongoing contribution of land-level change to reconstructed RSL change during the Common Era. To compare RSL reconstructions from different sites along the U.S. Atlantic coast and to identify climate-driven sea-level trends during the Common Era, we removed 0.9 mm/yr from the new Connecticut RSL reconstruction and used the EIV-IGP model to account for the covariance of age and vertical uncertainties introduced by this adjustment (Cahill et al., 2015). We assumed a constant rate of GIA over the 2200 yr duration of the reconstruction because this period is short relative to the adjustment time of the solid Earth to deglaciation. This analysis shows positive and negative departures from stable sea level (Fig. 8a). There was a slight sea-level rise of ~ 0.18 mm/yr at approximately 600–1000 CE. The rate of sea-level change fell to a minimum of -0.42 mm/yr at ~ 1400 CE (-0.22 to -0.62 mm/yr; 95% credible interval). The rate of sea-level rise

then accelerated continuously until reaching the current rate of 2.38 mm/yr (2.16–2.62 mm/yr; 95% credible interval), which is the fastest, century-scale rate in the past 2200 yrs. The compaction-free sea-level trend reconstructed at East River Marsh shows broad agreement with reconstructions from other sites in Connecticut including Hammock River Marsh (Thomas and Varekamp, 1991; van de Plassche et al., 1998; Varekamp et al., 1992).

To compare the new detrended sea-level reconstruction from Connecticut with others from elsewhere along the U.S. Atlantic coast, we applied the EIV-IGP and change-point models to existing records from New Jersey (Kemp et al., 2013a), North Carolina (Kemp et al., 2011), and Florida (Kemp et al., 2014). Change-point analysis shows a sharp and synchronous increase in the rate of sea-level rise that began in the 19th century with a common timing of 1865–1873 CE among the four records (Fig. 8). The global tide-gauge compilation of Church and White (2006, 2011) covers the period since 1870 CE and they noted that the acceleration of

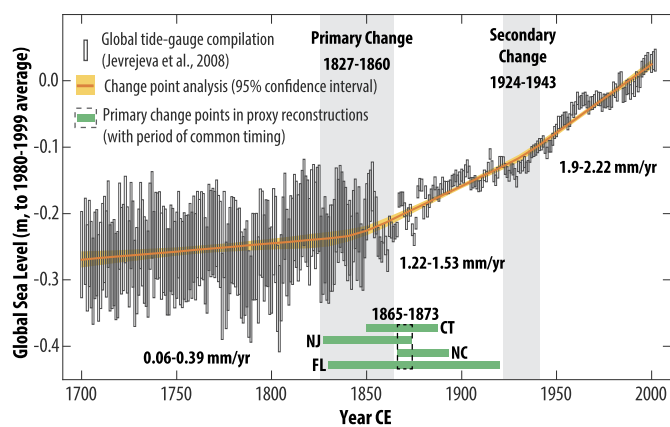


Fig. 9. Change point analysis of global mean sea level estimated from a compilation of global tide gauges. Annual estimates of global mean sea level are represented by boxes that incorporate vertical uncertainties reported by [Jevrejeva et al. \(2008\)](#) and a temporal uncertainty of ± 0.5 yrs. The mean and 95% credible interval of the change point regression are presented as a solid line and shaded envelope respectively. The timing of two change points (95% credible interval) are shown by vertical shaded areas. The linear rate of global mean sea level rise for periods defined by the change points are listed (95% credible interval). Labeled green bars indicate the timing of primary change points (95% credible interval) identified in proxy sea-level reconstructions from the U.S. Atlantic coast; the shared interval is 1865–1873 CE.

global sea-level rise commenced in the 19th century, with a secondary rate increase at ~ 1930 CE. This is supported by a recent reanalysis of the [Church and White \(2011\)](#) dataset, which shows global sea-level rise in excess of GIA at 1880 CE (>1 mm/yr) and a continuous acceleration to reach ~ 2 mm/yr at 2010 CE ([Cahill et al., 2015](#)). Similarly, [Hay et al. \(2015\)](#) demonstrated that the rate global mean sea-level was positive and increased throughout the 20th century. These findings indicate that sea-level rise on the U.S. Atlantic coast and globally began prior to ~ 1880 CE. The tide-gauge compilation of [Jevrejeva et al. \(2008\)](#) extends to 1700 CE, but prior to 1850 CE is based (out of necessity) only on records from Amsterdam, Liverpool, and Stockholm and therefore may not be representative of global trends. However, application of the change-point model to this record identified two intervals when the rate of sea-level rise increased ([Fig. 9](#)). The primary change occurred at 1827–1860 CE and there was a secondary increase at 1924–1943 CE. If the [Jevrejeva et al. \(2008\)](#) compilation is taken to represent global sea-level trends, then the difference in timing between the tide-gauge record (1827–1860 CE) and sea-level reconstructions (1865–1873 CE) suggests a short lag time between the onset of global sea-level rise and its detection in salt-marsh sediments along the U.S. Atlantic coast ([Fig. 9](#)). We contend that sea-level rise on the U.S. Atlantic coast accelerated in the late 19th century in response to global mean sea-level change. The reconstructions record the local to regional-scale expression of this global change caused by increased ocean mass and volume ([Church et al., 2013](#)). Departures from the global mean in the amount and rate of sea-level change may occur even after correction for GIA because of the static equilibrium (fingerprint) effect of ice melt (e.g. [Hay et al., 2014](#); [Mitrovica et al., 2001](#)) and simultaneous contributions from regional-scale processes such as ocean dynamics. The 19th century onset of accelerated sea-level rise contradicts the IPCC AR5, which concluded with high confidence that “rates of sea level rise exceeded the late Holocene background rate after about 1900” ([Masson-Delmonte et al., 2013](#)).

Two salt-marsh reconstructions from the United Kingdom did not definitively detect this acceleration ([Barlow et al., 2014](#); [Long et al., 2014](#)). This apparent absence is puzzling for two reasons. Firstly, it is present in the [Jevrejeva et al. \(2008\)](#) tide-gauge compilation which relies entirely on instrumental records from northern Europe (including the United Kingdom) prior to 1850 CE ([Fig. 9](#)).

Secondly, analysis of long tide-gauge records from the United Kingdom shows that 20th century rates of sea-level rise (e.g. [Woodworth et al., 2009](#)) exceeded long-term, GIA-driven regional trends (e.g. [Shennan and Horton, 2002](#)), indicating that the rate of sea-level rise increased (e.g. [Shennan and Woodworth, 1992](#)). A muted regional response to global mean sea-level change in the eastern North Atlantic and/or an exaggerated response to global mean sea-level change in the western North Atlantic could cause sea-level trends to differ across the Atlantic Ocean and for all proxy reconstructions to be accurate recorders of regional trends. In the United Kingdom, the average 20th century difference between GIA-driven background rates and those measured by tide-gauges was 1.4 ± 0.2 mm/yr ([Woodworth et al., 2009](#)). In comparison, estimates of global mean sea-level rise include 1.7 ± 0.2 mm/yr during the 20th century ([Church and White, 2011](#)) and 1.2 ± 0.2 mm/yr for 1901–1990 CE ([Hay et al., 2015](#)). The difference was ~ 1.9 mm/yr in Connecticut, New Jersey, and North Carolina and ~ 1.5 mm/yr in Florida ([Fig. 8](#)). Sea-level rise in the United Kingdom was similar to global estimates and we propose that large reconstruction uncertainties (approximately ± 0.4 m in Scotland and ± 0.3 m in the Isle of Wight record), and/or the insensitivity of minerogenic European salt marshes to accelerated sea-level change compared to their organogenic equivalents in North America prevented reliable detection of this feature of Common Era sea-level rise.

Prior to ~ 1800 CE, Common Era sea-level reconstructions support the conclusion of IPCC AR5 that “centennial-scale global mean sea-level variations did not exceed 25 cm over the past few millennia” ([Masson-Delmonte et al., 2013](#)). On millennial timescales, reconstructed trends are sensitive to the GIA correction applied, but the timing and direction (positive or negative) of centennial-scale departures from this long term trend are robust ([Fig. 8](#)). In Connecticut, there was a sea-level rise at ~ 600 –1000 CE with a maximum mean rate of 0.23 mm/yr and a sea level fall at ~ 1200 –1700 CE (maximum mean rate of -0.42 mm/yr). In New Jersey, there was a positive departure at ~ 300 –900 CE and a negative departure at ~ 1100 –1700 CE. The slight difference in timings between records could reflect the distribution of radiocarbon dates used to constrain the age-depth models. Similar patterns of change occurred in North Carolina, but they are asynchronous with those in New Jersey and Connecticut because the rise occurs at ~ 1000 –1400 CE, although there is some overlap in the timing of the fall, which occurs at ~ 1500 –1800 CE. There is no meaningful deviation from zero sea-level change in Florida until the onset of modern rates of rise. This pattern suggests that local- to regional-scale processes were the primary drivers of sea-level change along the U.S. Atlantic coast prior to the 19th century.

Sediment compaction could cause variability among reconstructions because the records from outside of Connecticut were developed from cores of high salt-marsh peat that varied in thickness from ~ 1.2 m in Florida to ~ 4.0 m in New Jersey. However, the coherence between New Jersey (most susceptible to compaction) and Connecticut (compaction-free) indicates that sediment compaction was not the primary cause of reconstructed spatial sea-level variability. Similarly, a geotechnical model estimated that sediment compaction contributed <0.03 m to the 1.4 m reconstructed RSL rise since ~ 1000 CE in North Carolina ([Brain et al., 2015](#)). Therefore, it is necessary to seek an alternative mechanism to explain the spatial differences among reconstructions.

On the U.S. Atlantic coast, the contrast in sea-level trends north and south of Cape Hatteras on instrumental ([Ezer et al., 2013](#); [McCarthy et al., 2015](#); [Yin and Goddard, 2013](#)) and Common Era timescales ([Kemp et al., 2014](#)) were partially attributed to changes in the strength and/or position of the Gulf Stream. The reconstruction from Connecticut supports this interpretation because of its coherence with New Jersey and their shared dissimilarity to

Florida prior to the 19th century. Proxy evidence from the Florida Strait indicates a ~ 3 Sv reduction in Gulf Stream strength during the Little Ice Age (at ~ 1350 – 1750 CE; Lund et al., 2006), which modeling studies suggest would cause a 1.5–6 cm sea-level rise north of Cape Hatteras (e.g. Kienert and Rahmstorf, 2012). This ocean dynamic effect could potentially offset sea-level fall from negative changes in ocean mass and volume caused by cooling temperatures. Climate reconstructions indicate that global temperature cooled from a peak of approximately $+0.1$ °C at ~ 950 CE to a minimum of -0.6 °C at ~ 1700 CE compared to the 1850–2006 CE average (Mann et al., 2008), although the timing and magnitude of cooling varied among continents with notable cold periods in North America centered on ~ 1650 CE and ~ 1850 CE (PAGES 2k Consortium, 2013). As temperatures cooled the rate of RSL rise in Connecticut and New Jersey fell below the rate of GIA at ~ 1100 – 1700 CE indicating that other processes were causing a sea-level fall. As temperatures rose after ~ 1700 CE, RSL rise in Connecticut and New Jersey once again exceeded GIA. This pattern and magnitude of Little Ice Age sea-level change likely resulted from the combined and simultaneous effects of cooling temperature (globally and in North America) and a weakening Gulf Stream. Further research (including additional sea-level records) is needed to distinguish and quantify the driving mechanisms of regional sea-level change prior to the 19th century.

6. Conclusions

We produced a compaction-free Common Era RSL reconstruction using salt-marsh sediment that accumulated directly on top of bedrock at East River Marsh, Connecticut. This sediment was exposed by excavating a trench and sampled to produce a suite of laterally and vertically ordered samples that preserve a record of salt-marsh ecosystems transgressing the evenly sloped bedrock outcrop in response to RSL rise. Paleomorph elevation was reconstructed with a transfer function trained on a regional-scale dataset of modern foraminifera and supported by bulk-sediment measurements of $\delta^{13}\text{C}$. A Bchron age-elevation model was constructed from radiocarbon dates and pollution markers of known age. The resulting ~ 2200 yr RSL reconstruction was combined with regional tide-gauge measurements and analyzed using an error-in-variables integrated Gaussian process model to quantify persistent Common Era sea-level trends with full consideration of uncertainty and the temporal distribution of data. After removing an estimated rate of glacio-isostatic adjustment, the compaction-free sea-level reconstruction shows a rise of ~ 0.18 mm/yr at ~ 600 – 1000 CE and a minimum rate of change (-0.42 mm/yr) at ~ 1400 CE. The current rate of rise (2.38 mm/yr) is the fastest century-scale rise of the last 2200 yrs and began at 1850–1886 CE, likely in response to global sea-level change. Prior to 1800 CE sea-level trends in Connecticut were similar to those in New Jersey, but dissimilar to those in Florida suggesting that regional-scale processes (specifically ocean dynamics) were the primary driver of sea-level change. Comparison with existing and reanalyzed RSL reconstructions at East River Marsh indicates that sediment compaction is not a major driver of RSL trends reconstructed using cores of salt-marsh sediment.

Acknowledgements

NOAA award NA11OAR4310101 and NSF grants EAR-1052848, EAR-0951686, and OCE-1154978 to BPH, JPD, ADH, and ACK supported this work. We thank Alex Wright and Orson van de Plassche for sharing their compilation of modern Connecticut foraminifera and understanding of Connecticut salt marshes. Christopher Maio, Richard Sullivan, Jim Cedeberg, Emmy Tsang, and Alan Nelson provided much-needed help in the field. Gabe Benoit and Helmut Ern-

stberger provided access to the DMA-80 and gamma counter. Vane publishes with the permission of the Director of the British Geological Survey. We thank Rosemarie Drummond and Dick Peltier for providing GIA predictions and Robin Edwards and two anonymous reviewers for their helpful comments and suggestions. This is a contribution to PALSEA2 and IGCP Project 588 “Preparing for Coastal Change”.

Appendix A. Supplementary material

Supplementary material related to this article can be found online at <http://dx.doi.org/10.1016/j.epsl.2015.07.034>.

References

- Balco, G., Briner, J., Finkel, R.C., Rayburn, J.A., Ridge, J.C., Schaefer, J.M., 2009. Regional beryllium-10 production rate calibration for late-glacial northeastern North America. *Quat. Geochronol.* 4, 93–107.
- Barlow, N.L.M., Long, A.J., Saher, M.H., Gehrels, W.R., Garnett, M.H., Scaife, R.G., 2014. Salt-marsh reconstructions of relative sea-level change in the North Atlantic during the last 2000 years. *Quat. Sci. Rev.* 99, 1–16.
- Bloom, A.L., 1964. Peat accumulation and compaction in Connecticut coastal marsh. *J. Sediment. Res.* 34, 599–603.
- Brain, M., Kemp, A.C., Horton, B.P., Culver, S.J., Parnell, A.C., Cahill, N., 2015. Quantifying the contribution of sediment compaction to late Holocene salt-marsh sea-level reconstructions, North Carolina, USA. *Quat. Res.* 83, 41–51.
- Brain, M.J., Long, A.J., Woodroffe, S.A., Petley, D.N., Milledge, D.G., Parnell, A.C., 2012. Modelling the effects of sediment compaction on salt marsh reconstructions of recent sea-level rise. *Earth Planet. Sci. Lett.* 345–348, 180–193.
- Cahill, N., Kemp, A.C., Horton, B.P., Parnell, A.C., 2015. Modeling sea-level change using errors-in-variables integrated Gaussian processes. *Ann. Appl. Stat.* 9, 547–571.
- Chmura, G.L., Aharon, P., 1995. Stable carbon isotope signatures of sedimentary carbon in coastal wetlands as indicators of salinity regime. *J. Coast. Res.* 11, 124–135.
- Church, J.A., Clark, P.U., Cazenave, A., Gregory, J.M., Jevrejeva, S., Levermann, A., Merrifield, M.A., Milne, G.A., Nerem, R.S., Nunn, P.D., Payne, A.J., Pfeffer, W.T., Stammer, D., Unnikrishnan, A.S., 2013. Sea-level change. In: Stocker, T.F., Qin, D., Plattner, G.K., Tignor, M., Allen, S.K., Boschung, J., Nauels, A., Xia, Y., Bex, V., Midgley, P.M. (Eds.), *Climate Change 2013: The Physical Science Basis. Contribution of Working Group I to the Fifth Assessment Report of the Intergovernmental Panel on Climate Change*. Cambridge University Press, pp. 1137–1216.
- Church, J.A., White, N.J., 2006. A 20th century acceleration in global sea-level rise. *Geophys. Res. Lett.* 33, L01602.
- Church, J.A., White, N.J., 2011. Sea-level rise from the late 19th to the early 21st century. *Surv. Geophys.* 32, 585–602.
- Dey, D., Ghosh, S.K., Mallick, B.K., 2000. *Generalized Linear Models: A Bayesian Perspective*. CRC Press.
- Donnelly, J.P., Cleary, P., Newby, P., Ettinger, R., 2004. Coupling instrumental and geological records of sea-level change: evidence from southern New England of an increase in the rate of sea-level rise in the late 19th century. *Geophys. Res. Lett.* 31, L05203.
- Edwards, R.J., Wright, A.J., van de Plassche, O., 2004. Surface distributions of salt-marsh foraminifera from Connecticut, USA: modern analogues for high-resolution sea level studies. *Mar. Micropaleontol.* 51, 1–21.
- Engelhart, S.E., Horton, B.P., Douglas, B.C., Peltier, W.R., Tornqvist, T.E., 2009. Spatial variability of late Holocene and 20th century sea-level rise along the Atlantic coast of the United States. *Geology* 37, 1115–1118.
- Engelhart, S.E., Peltier, W.R., Horton, B.P., 2011. Holocene relative sea-level changes and glacial isostatic adjustment of the U.S. Atlantic coast. *Geology* 39, 751–754.
- Ezer, T., Atkinson, L.P., Corlett, W.B., Blanco, J.L., 2013. Gulf Stream's induced sea level rise and variability along the U.S. mid-Atlantic coast. *J. Geophys. Res., Oceans* 118, 685–697.
- Gehrels, W.R., van de Plassche, O., 1999. The use of *Jadammina macrescens* (Brady) and *Balticammina pseudomacrescens* Brönnimann, Lutze and Whittaker (Protozoa: Foraminiferida) as sea-level indicators. *Palaeogeogr. Palaeoclimatol. Palaeoecol.* 149, 89–101.
- Gobeil, C., Tessier, A., Couture, R.-M., 2013. Upper Mississippi Pb as a mid-1800s chronostratigraphic marker in sediments from seasonally anoxic lakes in Eastern Canada. *Geochim. Cosmochim. Acta* 113, 125–135.
- Haslett, J., Parnell, A., 2008. A simple monotone process with application to radiocarbon-dated depth chronologies. *J. R. Stat. Soc., Ser. C, Appl. Stat.* 57, 399–418.
- Hay, C., Mitrovica, J.X., Gomez, N., Creveling, J.R., Austermann, J., Kopp, R.E., 2014. The sea-level fingerprints of ice-sheet collapse during interglacial periods. *Quat. Sci. Rev.* 87, 60–69.
- Hay, C., Morrow, E., Kopp, R.E., Mitrovica, J.X., 2015. Probabilistic reanalysis of twentieth-century sea-level rise. *Nature* 517, 481–484.

- Holsclaw, T., Sansó, B., Lee, H.K., Heitmann, K., Habib, S., Higdon, D., Alam, U., 2013. Gaussian process modeling of derivative curves. *Technometrics* 55, 57–67.
- Horton, B.P., 1999. The distribution of contemporary intertidal foraminifera at Cowpen Marsh, Tees Estuary, UK: implications for studies of Holocene sea-level changes. *Palaeogeogr. Palaeoclimatol. Palaeoecol.* 149, 127–149.
- Jevrejeva, S., Moore, J.C., Grinsted, A., Woodworth, P.L., 2008. Recent global sea level acceleration started over 200 years ago? *Geophys. Res. Lett.* 35, L08715.
- Johnson, B.J., Moore, K.A., Lehmann, C., Bohlen, C., Brown, T.A., 2007. Middle to late Holocene fluctuations of C₃ and C₄ vegetation in a Northern New England Salt Marsh, Sprague Marsh, Phippsburg Maine. *Org. Geochem.* 38, 394–403.
- Juggins, S., Birks, H.J.B., 2012. Quantitative environmental reconstructions from biological data. In: Birks, H.J.B., Lotter, A.F., Juggins, S., Smol, J.P. (Eds.), *Tracking Environmental Change Using Lake Sediments: Data Handling and Numerical Techniques*. Springer, pp. 431–494.
- Kemp, A.C., Bernhardt, C.E., Horton, B.P., Vane, C.H., Peltier, W.R., Hawkes, A.D., Donnelly, J.P., Parnell, A.C., Cahill, N., 2014. Late Holocene sea- and land-level change on the U.S. southeastern Atlantic coast. *Mar. Geol.* 357, 90–100.
- Kemp, A.C., Horton, B., Donnelly, J.P., Mann, M.E., Vermeer, M., Rahmstorf, S., 2011. Climate related sea-level variations over the past two millennia. *Proc. Natl. Acad. Sci.* 108, 11017–11022.
- Kemp, A.C., Horton, B.P., Vane, C.H., Corbett, D.R., Bernhardt, C.E., Engelhart, S.E., Anisfeld, S.C., Parnell, A.C., Cahill, N., 2013a. Sea-level change during the last 2500 years in New Jersey, USA. *Quat. Sci. Rev.* 81, 90–104.
- Kemp, A.C., Sommerfield, C.K., Vane, C.H., Horton, B.P., Chenery, S.R., Anisfeld, S.C., Nikitina, D., 2012a. Use of lead isotopes for developing chronologies in recent salt-marsh sediments. *Quat. Geochronol.* 12, 40–49.
- Kemp, A.C., Telford, R.J., Horton, B.P., Anisfeld, S.C., Sommerfield, C.K., 2013b. Reconstructing Holocene sea-level using salt-marsh foraminifera and transfer functions: lessons from New Jersey, USA. *J. Quat. Sci.* 28, 617–629.
- Kemp, A.C., Vane, C.H., Horton, B.P., Engelhart, S.E., Nikitina, D., 2012b. Application of stable carbon isotopes for reconstructing salt-marsh floral zones and relative sea level, New Jersey, USA. *J. Quat. Sci.* 27, 404–414.
- Kienert, H., Rahmstorf, S., 2012. On the relation between Meridional Overturning Circulation and sea-level gradients in the Atlantic. *Earth Syst. Dyn.* 3, 109–120.
- Lima, A.L., Bergquist, B.A., Boyle, E.A., Reuer, M.K., Dudas, F.O., Reddy, C.M., Eglinton, T.I., 2005. High-resolution historical records from Pettaquamscutt River basin sediments: 2. Pb isotopes reveal a potential new stratigraphic marker. *Geochim. Cosmochim. Acta* 69, 1813–1824.
- Long, A.J., Barlow, N.L.M., Gehrels, W.R., Saher, M.H., Woodworth, P.L., Scaife, R.G., Brain, M.J., Cahill, N., 2014. Contrasting records of sea-level change in the eastern and western North Atlantic during the last 300 years. *Earth Planet. Sci. Lett.* 388, 110–122.
- Lund, D.C., Lynch-Stieglitz, J., Curry, W.B., 2006. Gulf Stream density structure and transport during the last millennium. *Nature* 444, 601–604.
- Mann, M.E., Zhang, Z., Hughes, M.K., Bradley, R.S., Miller, S.K., Rutherford, S., Ni, F., 2008. Proxy-based reconstructions of hemispheric and global surface temperature variations over the past two millennia. *Proc. Natl. Acad. Sci.* 105, 13252–13257.
- Masson-Delmonte, V., Schulz, M., Abe-Ouchi, A., Beer, J., Ganopolski, A., González Rouco, J.F., Jansen, E., Lambeck, K., Luterbacher, J., Naish, T., Osborn, T., Otto-Bliesner, B., Quinn, T., Ramesh, R., Rojas, M., Shao, X., Timmermann, A., 2013. Information from paleoclimate archives. In: Stocker, T.F., Qin, D., Plattner, G.K., Tignor, M., Allen, S.K., Boschung, J., Nauels, A., Xia, Y., Bex, V., Midgley, P.M. (Eds.), *Climate Change 2013: The Physical Science Basis. Contribution of Working Group I to the Fifth Assessment Report of the Intergovernmental Panel on Climate Change*. Cambridge University Press, pp. 383–464.
- McCarthy, G.D., Haigh, I.D., Hirschi, J.J.M., Grist, J.P., Smeed, D.A., 2015. Ocean impact on decadal Atlantic climate variability revealed by sea-level observations. *Nature* 521, 508–510.
- Middleburg, J.J., Nieuwenhuize, J., Lubberts, R.K., van de Plassche, O., 1997. Organic carbon isotope systematics of coastal marshes. *Estuar. Coast. Shelf Sci.* 45, 681–687.
- Mitrovica, J.X., Tamisiea, M.E., Davis, J.L., Milne, G.A., 2001. Recent mass balance of polar ice sheets inferred from patterns of global sea-level change. *Nature* 409, 1026–1029.
- Nydic, K.R., Bidwell, A.B., Thomas, E., Varekamp, J.C., 1995. A sea-level rise curve from Guilford, Connecticut, USA. *Mar. Geol.* 124, 137–159.
- PAGES 2k Consortium, 2013. Continental-scale temperature variability during the past two millennia. *Nat. Geosci.* 6, 339–346.
- Parnell, A.C., Haslett, J., Allen, J.R.M., Buck, C.E., Huntley, B., 2008. A flexible approach to assessing synchronicity of past events using Bayesian reconstructions of sedimentation history. *Quat. Sci. Rev.* 27, 1872–1885.
- Peltier, W.R., 1996. Global sea level rise and glacial isostatic adjustment: an analysis of data from the east coast of North America. *Geophys. Res. Lett.* 23, GL00848.
- Peltier, W.R., Argus, D.F., Drummond, R., 2014. Space geodesy constrains ice-age terminal deglaciation: the ICE-6G_C (VM5a) model. *J. Geophys. Res., Solid Earth* 120, 450–487.
- Rasmussen, C.E., Williams, C.I.K., 2005. *Gaussian Processes for Machine Learning*. Massachusetts Institute of Technology Press.
- Redfield, A.C., Rubin, M., 1962. The age of salt marsh peat and its relation to recent changes in sea level at Barnstable, Massachusetts. *Proc. Natl. Acad. Sci. USA* 48, 1728–1735.
- Rowley, D.B., Forte, A.M., Moucha, R., Mitrovica, J.X., Simmons, N.A., Grand, S.P., 2013. Dynamic topography change of the eastern United States since 3 million years ago. *Science* 340, 1560–1563.
- Scott, D.B., Mediol, F.S., 1978. Vertical zonations of marsh foraminifera as accurate indicators of former sea levels. *Nature* 272, 528–531.
- Shennan, I., Horton, B., 2002. Holocene land- and sea-level changes in Great Britain. *J. Quat. Sci.* 17, 511–526.
- Shennan, I., Woodworth, P.L., 1992. A comparison of late Holocene and twentieth-century sea-level trends from the UK and North Sea region. *Geophys. J. Int.* 109, 96–105.
- Thomas, E., Varekamp, J., 1991. Paleo-environmental analysis of marsh sequences (Clinton, CT); evidence for punctuated sea-level rise during the latest Holocene. *J. Coast. Res.* 11, 125–158.
- van de Plassche, O., 1991. Late Holocene sea-level fluctuations on the shore of Connecticut inferred from transgressive and regressive overlap boundaries in salt-marsh deposits. *J. Coast. Res.* 11, 159–179.
- van de Plassche, O., van der Borg, K., de Jong, A.F.M., 1998. Sea level-climate correlation during the past 1400 yr. *Geology* 26, 319–322.
- Vane, C.H., Chenery, S.R., Harrison, I., Kim, A.W., Moss-Hayes, V., Jones, D.G., 2011. Chemical signatures of the Anthropocene in the Clyde estuary, UK: sediment-hosted Pb, ^{207/206}Pb, total petroleum hydrocarbon, polyaromatic hydrocarbon and polychlorinated biphenyl pollution records. *Philos. Trans. R. Soc. A, Math. Phys. Eng. Sci.* 369, 1085–1111.
- Varekamp, J., Kreulen, B., ten Brink, B.M., Mecray, E., 2003. Mercury contamination chronologies from Connecticut wetlands and Long Island Sound sediments. *Environ. Geol.* 43, 268–282.
- Varekamp, J., Thomas, E., van de Plassche, O., 1992. Relative sea-level rise and climate change over the last 1500 years. *Terra Nova* 4, 293–304.
- Woodworth, P.L., Teferle, F.N., Bingley, R.M., Shennan, I., Williams, S.D.P., 2009. Trends in UK mean sea level revisited. *Geophys. J. Int.* 176, 19–30.
- Wright, A.J., Edwards, R.J., van de Plassche, O., 2011. Reassessing transfer-function performance in sea-level reconstruction based on benthic salt-marsh foraminifera from the Atlantic coast of NE North America. *Mar. Micropaleontol.* 81, 43–62.
- Yin, J., Goddard, P.B., 2013. Oceanic control of sea level rise patterns along the East coast of the United States. *Geophys. Res. Lett.* 40, 5514–5520.